Friction, Frontogenesis, and the Stratification of the Surface Mixed Layer

LEIF THOMAS*

Department of Physical Oceanography, Woods Hole Oceanographic Institution, Woods Hole, Massachusetts

RAFFAELE FERRARI

Massachusetts Institute of Technology, Boston, Massachusetts

(Manuscript received 11 March 2007, in final form 8 May 2008)

ABSTRACT

The generation and destruction of stratification in the surface mixed layer of the ocean is understood to result from vertical turbulent transport of buoyancy and momentum driven by air–sea fluxes and stresses. In this paper, it is shown that the magnitude and penetration of vertical fluxes are strongly modified by horizontal gradients in buoyancy and momentum. A classic example is the strong restratification resulting from frontogenesis in regions of confluent flow. Frictional forces acting on a baroclinic current either imposed externally by a wind stress or caused by the spindown of the current itself also modify the stratification by driving Ekman flows that differentially advect density. Ekman flow induced during spindown always tends to restratify the fluid, while wind-driven Ekman currents will restratify or destratify the mixed layer if the wind stress has a component up or down front (i.e., directed against or with the geostrophic shear), respectively. Scalings are constructed for the relative importance of friction versus frontogenesis in the restratification of the mixed layer and are tested using numerical experiments of mixed layer fronts forced by both winds and a strain field. The scalings suggest and the numerical experiments confirm that for wind stress magnitudes, mixed layer depths, and cross-front density gradients typical of the ocean, wind-induced friction often dominates frontogenesis in the modification of the stratification of the upper ocean. The experiments reveal that wind-induced destratification is weaker in magnitude than restratification because the stratification generated by up-front winds confines the turbulent stress to a depth shallower than the Ekman layer, which enhances the frictional force, Ekman flow, and differential advection of density. Frictional destratification is further reduced over restratification because the stress associated with the geostrophic shear at the surface tends to compensate a down-front wind stress.

1. Introduction

The surface mixed layer of the ocean is a weakly stratified layer often encountered below the air–sea interface, where turbulent mixing is strong in response to atmospheric forcing. The processes that set the stratification and ventilation of the mixed layer are an essential part of the coupled climate system, because this layer regulates the exchange of heat, freshwater, and all other climatically relevant tracers between the atmosphere and the ocean. Traditional models assume that the vertical structure of the mixed layer is set by the vertical mixing of buoyancy and momentum driven by atmospheric surface fluxes and stresses. Lapeyre et al. (2006) and Fox-Kemper et al. (2008) have recently pointed out that during times of weak air–sea fluxes, lateral dynamics become leading order and tend to restratify the mixed layer through ageostrophic slumping of lateral buoyancy gradients. The goal of this paper is to extend recent work of Thomas (2005) and show that frictional forces acting on buoyancy fronts can also modify the stratification of the mixed layer. These effects are currently ignored in models and theory of the upper ocean and are likely to introduce biases in our understanding of ocean–atmosphere interactions.

Most studies of the ocean mixed layer are cast in terms of the impact of air–sea fluxes on the momentum

* Current affiliation: Department of Environmental Earth System Science, Stanford University, Stanford, California.

Corresponding author address: Raffaele Ferrari, Department of Earth Atmospheric and Planetary Sciences, 54–1420, Massachusetts Institute of Technology, 77 Mass. Ave., Cambridge, MA 02139.
E-mail: rferrari@mit.edu

DOI: 10.1175/2008JPO3797.1

and buoyancy budgets. Less attention has been paid to the potential vorticity (PV) budget. However, potential vorticity is an extremely useful tracer to study the dynamics of rotating stratified fluids. First, potential vorticity can only be changed by diabatic heating/cooling or friction. The amount of potential vorticity possessed by a water mass in the ocean is therefore a convenient way of tagging it, unaffected by changes of depth, latitude, or shear. Second, potential vorticity distributions strongly constrain the large-scale circulation through the "invertibility principle." The invertibility principle states that if the total mass under each isentropic surface is specified, then knowledge of the global distribution of potential vorticity on each isentropic surface together with boundary conditions is sufficient to deduce all other dynamical fields, such as currents, stratification, geopotential heights, and so forth. Third, potential vorticity is generated and destroyed through diabatic and frictional processes mediated by velocity shears and buoyancy gradients. Hence, the potential vorticity budget provides a natural framework to study the interaction of air–sea fluxes and lateral fronts in setting the stratification of a fluid.

Heating and cooling generate and destroy potential vorticity at the ocean surface and modify the stratification. Haine and Marshall (1998) show that the destruction of potential vorticity during cooling events can be associated with residual vertical stratification in the presence of lateral density gradients. Hence, potential vorticity is a more natural variable than stratification to describe the dynamics of the mixed layer. Lapeyre et al. (2006) show that restratification at an outcropping ocean front can also be conveniently described in terms of potential vorticity. They consider an idealized front with no-flux and free-slip surface boundary conditions to minimize nonconservative processes. Under such conditions, the potential vorticity of the fluid is conserved and restratification occurs through a rearrangement of potential vorticity through surface frontogenesis: a frontogenetic strain field drives a thermally direct secondary circulation that increases the stratification even in a fluid with a spatially homogeneous PV field (Hoskins and Bretherton 1972).

In this paper, it is shown that in the real ocean, friction can also modify the potential vorticity of the mixed layer and hence modify the stratification of the upper ocean. The frictional generation–destruction of potential vorticity has two contributions: PV change induced by frictional forces with curl, which induce Ekman vertical stretching of isopycnals, and baroclinic generation due to horizontal Ekman flows advecting light fluid over dense, or vice versa, at lateral buoyancy gradients. The baroclinic generation has not been given much attention in the oceanographic literature, but it is known to play an important role at atmospheric fronts (Cooper et al. 1992; Davis et al. 1993; Adamson et al. 2006). Using simple scaling arguments and numerical experiments, it is shown that the modification of the stratification by these potential vorticity sources–sinks is as strong or exceeds that associated with frontogenesis. Furthermore, it is emphasized that restratification–destratification by frontogenesis and friction is most efficient in the surface mixed layer with a weaker effect in the main thermocline.

2. Governing equations for changes in the mixed layer stratification

The average stratification over a rectangular volume of widths L_x, L_y in the x and y directions and bounded by the vertical levels z_t and z_b is

$$\overline{N^2} \equiv \frac{1}{H}\int_{z_b}^{z_t} \partial_z\langle b\rangle\, dz = \frac{\langle b\rangle|_{z=z_t} - \langle b\rangle|_{z=z_b}}{H}, \quad (1)$$

where $b = -g\rho/\rho_o$ is the buoyancy, $\langle\ \rangle = (L_xL_y)^{-1}\int_{-L_x/2}^{L_x/2}\int_{-L_y/2}^{L_y/2} dx\, dy$ denotes the lateral average, and $H = z_t - z_b$. The buoyancy equation

$$\partial_t b + \mathbf{u}_h\cdot\nabla b + w\partial_z b = \mathcal{D} \quad (2)$$

(where term $\mathcal{D}$ encompasses all diabatic processes and subscript h signifies a horizontal velocity vector) can be laterally averaged to yield an equation governing the rate of change of the average stratification:

$$\partial_t\overline{N^2} = -\frac{1}{H}\langle\mathbf{u}_h\cdot\nabla b\rangle\Big|_{z=z_b}^{z=z_t} - \frac{1}{H}\langle w\partial_z b\rangle\Big|_{z=z_b}^{z=z_t} + \frac{1}{H}\langle\mathcal{D}\rangle|_{z=z_b}^{z=z_t}. \quad (3)$$

This equation states that the average stratification of a water column can be modified through diabatic irreversible processes, differential horizontal advection of buoyancy, or vertical advection of buoyancy.

As described in Lapeyre et al. (2006), an alternative equation for the rate of change of $\overline{N^2}$ can be derived from the potential vorticity equation

$$\partial_t q = -\nabla\cdot\mathbf{J}, \quad (4)$$

where $\mathbf{q} = \nabla\cdot(\boldsymbol{\omega}_a b)$ is the Ertel PV, $\boldsymbol{\omega}_a = f\hat{z} + \nabla\times\mathbf{u}$ is the absolute vorticity, and $\mathbf{J}$ is the PV flux. The PV flux

$$\mathbf{J} = \mathbf{u}q + \nabla b\times\mathbf{F} - \boldsymbol{\omega}_a\mathcal{D} \quad (5)$$

has an advective component $\mathbf{u}q$ and a nonadvective component that arises from diabatic processes and from frictional and nonconservative body forces $\mathbf{F}$ (Marshall

and Nurser 1992). Calculating the volume average of (4) over the same rectangular volume used in (3), utilizing Gauss's theorem, and assuming that the horizontal flow at the lateral boundaries of the volume goes to zero or is periodic yields the alternative equation for the rate of change of $\overline{N^2}$

$$\partial_t \overline{N^2} = -\frac{1}{fH}\left(\underbrace{\partial_t \langle \zeta b\rangle|_{z=z_b}^{z=z_t}}_{\text{FRONT}} + \underbrace{\langle wq\rangle|_{z=z_b}^{z=z_t}}_{\text{ADV}} + \underbrace{\langle J_z^F\rangle|_{z=z_b}^{z=z_t}}_{\text{FRIC}} + \underbrace{\langle J_z^{\mathcal{D}}\rangle|_{z=z_b}^{z=z_t}}_{\text{DIA}}\right), \tag{6}$$

where

$$J_z^F \equiv (\boldsymbol{\nabla}_h b \times \mathbf{F}_h)\cdot \hat{\mathbf{z}} \tag{7}$$

and

$$J_z^{\mathcal{D}} \equiv -(f+\zeta)\mathcal{D} \tag{8}$$

are the vertical components of the frictional and diabatic PV fluxes, respectively, and $\zeta \equiv \partial_x v - \partial_y u$ is the vertical vorticity.

Equation (6) highlights the various phenomena that can result in restratification (or destratification) of the ocean: frontogenesis or frontolysis (FRONT), advection of PV (ADV), friction (FRIC), and diabatic processes (DIA). If the vertical levels z_t and z_b do not intersect surface and benthic boundary layers, then advection of PV through the bounding surfaces dominates over the other three terms: diabatic and frictional effects are weak away from boundaries, while FRONT scales like ADV times a Rossby number. In the ocean interior mean and eddy motions are close to geostrophic balance, Rossby numbers are small and FRONT $\ll$ ADV. The relative strengths of FRIC and DIA were explored in Thomas (2005), who showed that at wind-forced ocean fronts, frictional PV change can be at least as strong as diabatic creation–destruction of PV–stratification for typical air–sea buoyancy and momentum fluxes and cross-front density gradients.

The effect of frontogenesis/frontolysis on the modification of the stratification can be isolated by considering an adiabatic, frictionless flow, where $w = 0$ at $z = z_t, z_b$. Comparing (3) and (6) in this limit yields

$$\text{FRONT} = f\langle \mathbf{u}_h \cdot \boldsymbol{\nabla} b\rangle|_{z=z_b}^{z=z_t}. \tag{9}$$

This result highlights the importance of differential horizontal advection in re–de-stratification by frontogenesis–frontolysis. Indeed, in the classic work of Hoskins and Bretherton (1972), where the connection between frontogenesis and restratification was established, it was demonstrated that frontogenetic confluent (frontolytic diffluent) flow will always drive a thermally direct (indirect) ageostrophic secondary circulation whose horizontal velocity tends to flatten (steepen) isopycnals.

At the ocean top and bottom boundaries all four terms in the right-hand side of Eq. (6) participate in restratification (or destratification). The relation between surface frontogenesis and restratification is investigated in Lapeyre et al. (2006), who use numerical simulations to diagnose how frontogenetic convergent flows generate correlations between buoyancy and vertical vorticity, which through the term FRONT increases the stratification. It is fairly obvious to see how advection of PV and diabatic processes can result in changes of PV (e.g., upwelling of high PV from the stratified pycnocline and surface heating will both result in restratification of the mixed layer), but it is not immediately transparent why friction should change the average stratification. Indeed, when comparing Eqs. (3) and (6), the apparent lack of influence of friction on the stratification in (3) led Lapeyre et al. (2006) to conclude that while friction might change the PV, its effect is felt on the vertical vorticity but does not directly contribute to restratification. It will be demonstrated in the next section that this conclusion is not generally true and that surface friction can contribute significantly to both restratification and destratification of the mixed layer.

3. Modification of stratification by friction

A frictional force in the surface boundary layer will induce an Ekman flow that can modify the stratification. While frictional forces appear in the formulation based on the PV budget in (6), they do not appear explicitly in the more traditional budget in (3). To illustrate how friction enters in (3), the horizontal velocity can be decomposed into two parts: $\mathbf{u}_h = \mathbf{u}_{\text{nf}} + \mathbf{u}_e$, that is, one associated with all nonfrictional processes such as frontogenesis ($\mathbf{u}_{\text{nf}}$) and the other with Ekman flow. The Ekman flow is related to the frictional force as $\mathbf{u}_e = \mathbf{F}_h \times \hat{\mathbf{z}}/f$. Substituting this expression into (3), it is found that the contribution to the horizontal differential advection by the Ekman flow is proportional to the frictional PV flux

$$-\frac{1}{H}\langle \mathbf{u}_e \cdot \boldsymbol{\nabla} b\rangle|_{z=z_b}^{z=z_t} = -\frac{1}{fH}\langle \mathbf{F}_h \times \hat{\mathbf{z}} \cdot \boldsymbol{\nabla} b\rangle|_{z=z_b}^{z=z_t} = -\frac{1}{fH}\langle J_z^F\rangle|_{z=z_b}^{z=z_t}. \tag{10}$$

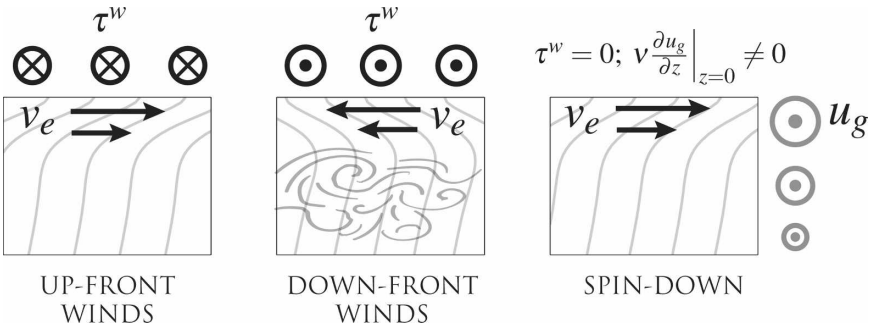

FIG. 1. Schematic illustrating frictional re–de-stratification at a baroclinic current in the upper ocean. (left) Up-front winds blowing against a baroclinic geostrophic flow u_g will drive an Ekman flow v_e that flattens isopycnals (gray) and hence restratifies the fluid via differential horizontal advection of buoyancy. (middle) When the wind is oriented down front, Ekman advection of buoyancy destabilizes the water column, driving convective mixing and a reduction of the stratification. (right) With no wind forcing, the frictional spindown of a baroclinic current arising from the mismatch of the geostrophic shear and the zero stress boundary condition induces a restratifying Ekman flow.

Owing to Ekman advection of buoyancy, friction once again explicitly appears in the equation for the stratification in terms of the frictional PV flux (7).

The manner by which differential advection of buoyancy by Ekman flow, and equivalently vertical frictional PV fluxes, modify the stratification of the surface mixed layer is illustrated in Fig. 1. Friction can either input or extract PV from the fluid, depending on the orientation of the frictional force and the lateral buoyancy gradient. For wind-forced flows, the frictional force at the sea surface is dominantly in the direction of the wind stress. Down front winds (i.e., oriented in the direction of the baroclinic shear) drive vertical frictional PV fluxes that extract PV from the ocean. For these winds, Ekman flow advects denser water over light, and convection ensues that mixes the stratification and reduces the PV (Thomas 2005). Friction injects PV into the fluid when a baroclinic current is forced by up front winds because the Ekman flow advects lighter water over dense and restratifies the fluid.

Even without wind forcing, frictional spindown will modify the stratification of baroclinic geostrophic currents. In this case, the turbulent stress at the surface must be zero, that is, $(\tau_x, \tau_y) = 0$ at $z = 0$; however, the geostrophic shear and the stress associated with that shear, $\rho_o \nu\ (\partial_z u_g, \partial_z v_g)$ (ν is an eddy viscosity and $\mathbf{u}_g$ is the geostrophic flow), is nonzero. Because the geostrophic flow does not satisfy the no-stress boundary condition, an Ekman flow must be induced to cancel the geostrophic shear at the surface:

$$\rho\nu(\partial_z u_e|_{z=0}, \partial_z v_e|_{z=0}) = -\rho\nu(\partial_z u_g|_{z=0}, \partial_z v_g|_{z=0}) \equiv (\tau_x^g, \tau_y^g) \quad (11)$$

(Garrett and Loder 1981; Thompson 2000). As described in Thomas and Rhines (2002), this Ekman flow that acts to spin down the geostrophic current can be thought as being driven by an effective "geostrophic stress" (τ_x^g, τ_y^g) that is directed opposite to the geostrophic shear. The Ekman transport is therefore always directed down the buoyancy gradient; hence, advection of buoyancy by the Ekman flow tends to stratify the fluid (Fig. 1). As shown in (10), the rate at which this restratification occurs is proportional to the frictional PV flux. An expression for the frictional PV flux induced during spindown can be derived using the Ekman spiral solution, which satisfies boundary condition (11), and is given by $\langle J_z^F \rangle|_{z=0} = -1/2 \langle \delta_e |\nabla_h b|^2 \rangle|_{z=0}$, where $\delta_e = \sqrt{2\nu/f}$ is the depth of the Ekman layer. The frictional PV flux during spindown is a negative definite quantity that results in the increase of both the PV and stratification of the fluid. Notice that if there is no lateral shear in the geostrophic flow, the geostrophic stress and frictional force are horizontally uniform and hence do not modify the vertical vorticity (the same is true if such a geostrophic flow were forced by a spatially uniform wind stress). This demonstrates that friction can change the PV of the fluid by modifying the stratification rather than the vertical vorticity.

4. Modification of stratification by frontogenesis

Whether frictional restratification and destratification of the surface Ekman layer is of leading-order importance in upper ocean dynamics depends on how large the contribution of friction is compared to surface frontogenesis, diabatic processes, and vertical advec-

tion in (6). In this section, classic results on frontogenetic restratification are reviewed. A comparison of the various processes on the upper ocean stratification is the focus of the next section.

Equation (9) shows that the rate of change of stratification due to frontogenesis–frontolysis is controlled by the differential horizontal advection at the top and bottom of the front. A scaling for this ageostrophic secondary circulation (ASC) is obtained from the two-dimensional quasigeostrophic approximate version of the Eliassen–Sawyer equation for the ageostrophic streamfunction ψ:

$$f^2\partial_{zz}\psi + N^2\partial_{yy}\psi = -2Q_2, \tag{12}$$

where $(v_{ag}, w) = (\partial_z\psi, -\partial_y\psi)$ and

$$Q_2 = -\frac{\partial \mathbf{u}_g}{\partial y}\cdot\boldsymbol{\nabla}_h b \tag{13}$$

is a component of the "Q vector" introduced by Hoskins et al. (1978), which drives a thermally direct ASC (v_{ag}, w) in frontogenetic conditions. Taking the volume integral of (12) over the rectangular control volume described in section 2 with $z_t = 0$ and $z_b = -H$, and using Gauss's theorem, yields

$$L_xL_y\langle\partial_z\psi\rangle|_{z_b=-H}^{z_t=0} + \int_{-L_x/2}^{L_x/2}\int_{-H}^{0}\partial_{y_*}\psi|_{y=-L_y/2}^{y=L_y/2} = -L_xL_yH\frac{2}{f^2}\overline{Q_2}, \quad \text{where } y_* = (f/N)y. \tag{14}$$

Let us assume that the region of enhanced frontal gradients in the fluid is finite, so that the geostrophic forcing Q_2 is confined to a region in y of width L_f. If the meridional edges of the control volume are far away from the frontal region (i.e., $L_y \gg L_f$), then $\partial_{y_*}\psi|_{y=-L_y/2}^{y=L_y/2} \approx 0$ and the second term on the left-hand side of (14) can be neglected. If we also choose the bottom surface of the control volume to coincide with a depth H representative of the vertical length scale of the frontogenesis-driven ASC, then (14) can be used to calculate the difference in mean horizontal velocity between $z_t = 0$ and $z_b = -H$,

$$\Delta v_{\text{front}} \equiv \langle\partial_z\psi\rangle|_{z_b=-H}^{z_t=0} = -H\frac{2}{f^2}\overline{Q_2}$$

$$= H\frac{2}{f}\overline{(\partial_y u_g\partial_z v_g - \partial_y v_g\partial_z u_g)}. \tag{15}$$

The change in the geostrophic flow over the depth H scales as $H|\partial_z\mathbf{u}_g| = \Delta u_g$, so an appropriate scaling for the drop in velocity (15) is

$$\Delta v_{\text{front}} \sim \text{Ro}\Delta u_g \tag{16}$$

where the lateral shear $\partial_y u_g$ and confluence $-\partial_y v_g$ of the geostrophic flow averaged over the control volume have been assumed to scale as f times a bulk Rossby number, Ro. Notice that Ro characterizes the strain flow that drives frontogenesis and not the large Rossby number motions that develop as a result of frontogenesis.

5. Scalings for the relative contributions of friction and frontogenesis to modifications of stratification

Expressions (9) and (10) show that the relative contributions of friction and frontogenesis to changes in stratification, governed by (6), are determined by the relative drop in horizontal velocities over the front vertical scale associated with frictional processes and frontogenesis, respectively, that is,

$$\frac{\text{FRIC}}{\text{FRONT}} \equiv \gamma \sim \frac{\Delta v_{\text{fric}}}{\Delta v_{\text{front}}}. \tag{17}$$

In this section, scalings for the horizontal flows associated with friction Δv_{fric} will be derived and used to estimate this ratio.

Frictionally driven flows are largest at the surface and decay to zero over the Ekman layer depth. A scaling for the surface horizontal flow associated with spindown Δv_{sd} and wind forcing Δv_{wind} is given by Ekman solutions:

$$\Delta v_{\text{fric}} \sim \underbrace{\frac{\tau^g}{\rho_o f\delta_e}}_{\Delta v_{\text{sd}}} + \underbrace{\frac{\tau^w}{\rho_o f\delta_e}}_{\Delta v_{\text{wind}}}, \tag{18}$$

where τ^g and τ^w are representative values for the geostrophic stress and the component of the wind stress parallel or antiparallel to the frontal jet. A scaling for the drop in velocity associated with frontogenesis is given by (16), that is, $\Delta v_{\text{front}} \sim \text{Ro}\Delta u_g$.

The scalings (18) and (16) can now be used to estimate the ratio in (17). Considering the frictional flows driven by spindown and wind stress separately, then the ratio for spindown is

$$\gamma_{\text{sd}} \equiv \frac{\Delta v_{\text{sd}}}{\Delta v_{\text{front}}} = \frac{\tau^g}{\rho_o f\delta_e\text{Ro}\Delta u_g}. \tag{19}$$

In spindown problems, the stress at the surface is proportional to the vertical shear through an eddy viscosity as in (11), and the Ekman layer thickness is given by

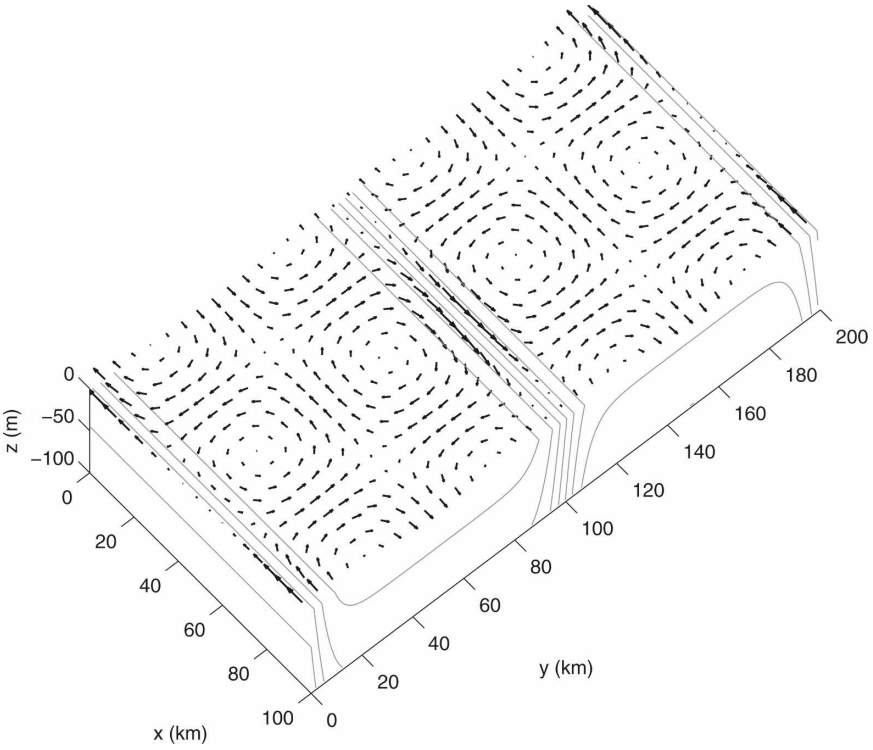

FIG. 2. Initial condition for the numerical simulations. Density is contoured in gray and the velocity vectors of the flow at the surface are shown in black.

$\delta_e = \sqrt{2\nu/f}$. The Ekman flow driven by the geostrophic shear therefore scales as $\tau^g/\rho_o f\delta_e \sim (\delta_e/H)\Delta u_g$; hence

$$\gamma_{\rm sd} \sim {\rm Ek}^{1/2}{\rm Ro}^{-1}, \tag{20}$$

where ${\rm Ek} = \delta_e^2/H^2$ is the Ekman number. When friction is very weak, like in the simulations of Lapeyre et al. (2006) (they use $\nu = 10^{-5}$ m^2 s^{-1}), $\delta_e \ll H$ and frontogenesis dominates the restratification process.

When a stress is applied at the ocean surface, the Ekman layer thickness is given by $\delta_e = 0.4u^*/f$, where $u^* = \sqrt{\tau^w/\rho_o}$ is the friction velocity and τ is the stress at the surface (Wimbush and Munk 1970). These relationships can be used to calculate the relative contribution to mixed layer restratification by frontogenesis and frictionally induced flows,

$$\gamma_{\rm wind} \equiv \frac{\Delta\nu_{\rm wind}}{\Delta\nu_{\rm front}} \sim \frac{u_w^*}{\Delta u_g}{\rm Ro}^{-1}, \tag{21}$$

where $u_w^* = \sqrt{\tau^w/\rho_o}$. The friction velocity for a typical wind stress of 0.1 N m^{-2} is $u_w^* \sim 0.01$ m s^{-1}, so that even in a relatively strong baroclinic current with $\Delta u_g =$ 0.1 m s^{-1} and Ro = 0.1, $\gamma_{\rm wind} \sim 1$. This scaling argument suggests that winds, in typical oceanic conditions, are as important as frontogenesis for modifying the stratification in the mixed layer.

In the next section, numerical simulations designed to pit restratification by frontogenesis against frictional destruction and creation of PV, which were used to test the above scaling arguments, are described.

6. Numerical experiments

a. Configuration of experiments

The configuration of the experiments is designed to isolate the effects of frontogenesis and friction and deemphasize the role of vertical advection in the modification of mixed layer stratification. To accomplish this, the model domain is confined to a layer of thickness $D = 100$ m, and the vertical velocity and advective flux of PV, ADV in (6), are both zero at the bottom. The initial density field used in the simulations is characterized by two isolated fronts with a spatially uniform background stratification (Fig. 2). An analytical form for the initial condition of the density that incorporates these features is

$$\rho(y, z) = \Delta\rho_y Y(y) - \frac{\rho_o}{g}N_o^2 z, \tag{22}$$

where

$$Y(y) = \begin{cases} 0.5\left[1 - \tanh\left(\dfrac{y}{L_f}\right) + \tanh\left(\dfrac{y - \mathcal{L}_y/2}{L_f}\right)\right] & 0 \le y \le \mathcal{L}_y/2, \\ 0.5\left[\tanh\left(\dfrac{y - \mathcal{L}_y/2}{L_f}\right) - \tanh\left(\dfrac{y - \mathcal{L}_y}{L_f}\right) - 1\right] & \mathcal{L}_y/2 \le y \le \mathcal{L}_y, \end{cases} \quad (23)$$

and $N_o^2 = 5 \times 10^{-6}\ \mathrm{s}^{-2}$ is the background stratification. The frontal width, $L_f = 8$ km, and the north–south and east–west extent of the domain, $\mathcal{L}_y = 200$ km and $\mathcal{L}_x = 100$ km, are the same for all the experiments. Periodic boundary conditions are imposed on all variables on the northern, southern, eastern, and western boundaries of the domain. All experiments, excluding one, have a horizontal resolution, $\Delta x = \Delta y$, of 1 km. One experiment was performed with an enhanced horizontal resolution of $\Delta x = \Delta y = 500$ m. The vertical resolution of the model, Δz, is uniform and equal to 5.3 m. The fluid is on an f plane with the Coriolis parameter set to $f = 1 \times 10^{-4}\ \mathrm{s}^{-1}$; consequently, the density field is associated with a geostrophically balanced zonal flow. Given the Coriolis parameter, background stratification, and depth of the mixed layer used in the simulations, the mixed layer Rossby radius of deformation, $N_o D/f = 2.2$ km, is resolved in the numerical experiments.

The experiments are forced by a combination of strain associated with a barotropic velocity field inserted into the flow as an initial condition and by a spatially uniform wind stress, τ_x^w, oriented in the positive x direction. The barotropic velocity field is given by the streamfunction

$$\Phi = \alpha \frac{\mathcal{L}_x \mathcal{L}_y}{8\pi^2} \cos\left(\frac{2\pi}{\mathcal{L}_x} x\right) \sin\left[\frac{4\pi}{\mathcal{L}_y}\left(y - \frac{\mathcal{L}_y}{2}\right)\right], \quad (24)$$

where the velocity is equal to $\nabla\Phi \times \hat{\mathbf{z}}$, and α is the maximum value of the confluence. At $t = 0$, the barotropic flow is superposed on the baroclinic geostrophic flow of the mixed layer fronts, resulting in the velocity field shown in Fig. 2. At the fronts, confluence (diffluence) is centered at $x = \mathcal{L}_x/4$ ($x = 3\mathcal{L}_x/4$). The wind stress is applied at the start of each simulation and kept at a constant value through the length of the experiment. The bottom stress follows a quadratic drag law with a drag coefficient of 1×10^{-8}, which was chosen to be extremely small to minimize the Ekman flow in the bottom boundary layer.

Vertical mixing of momentum and tracers is attained through the K-profile parameterization (KPP) mixing scheme of Large et al. (1994). To avert frontal collapse, biharmonic friction and diffusion are used, with mixing coefficients equal to $6 \times 10^7\ \mathrm{m}^4\ \mathrm{s}^{-1}$ and $3.8 \times 10^6\ \mathrm{m}^4\ \mathrm{s}^{-1}$ for the lower- and higher-resolution runs, respectively. Advection of tracers is accomplished using the recursive flux-corrected MPDATA advection scheme of Smolarkiewicz and Margolin (1998) to suppress under–overshooting of density that tends to occur in frontogenetic situations. A third-order upstream-biased advection scheme is implemented for momentum.

A total of 18 experiments were performed, each lasting 10 inertial periods, a duration long enough for the development of frontogenesis. The key parameters of the problem ($\Delta\rho_y$, α, and τ_x^w) that were varied in each experiment are listed in Table 1. The confluence α used in the experiments spans 0–0.25f and was chosen to represent horizontal strain typical of mixed layer eddies. The range of cross-front density contrasts employed in the runs corresponds to lateral buoyancy gradients of $0.66–3.0 \times 10^{-7}\ \mathrm{s}^{-2}$ at $t = 0$, which fall on the high end of frontal gradients in the ocean. The experiments are forced by weak to moderately strong wind stresses of magnitude 0–0.25 N m^{-2}. Given these parameters, the scaling γ_{wind} ranges from 0.21 to 6.7 (excluding the wind-only and frontogenesis-only runs). Therefore, these experiments cover both the frontogenetically and frictionally dominant regimes of mixed layer re/destratification.

b. Basic properties of the numerical solutions

To illustrate the basic properties of the numerical experiments, the evolution of the density field in run 4 is plotted in Figs. 3–5. Run 4 is chosen as a control case because the frictional and frontogenetic forcings used in the experiment are predicted to have a comparable effect on the mixed layer stratification, because using the scaling in (21) $\gamma_{\mathrm{wind}} = 0.67 \approx 1$.

The evolution of the surface density field reveals that frontal intensification occurs in the experiments (Fig. 3). Frontogenesis driven by the confluent barotropic flow dominates over frontolysis associated with the diffluent flow, resulting in a net strengthening of the zonally averaged cross-front density gradient. Wind forcing leads to a southward translation of both fronts, with the front to the north experiencing a larger displacement.

To ascertain the effect that wind forcing has on the mixed layer stratification, the zonally averaged density fields for runs 3 (which was forced by strain only, not winds) and 4 (which was forced by strain and a mod-

TABLE 1. Experimental parameters for numerical simulations, i.e., the cross-front density contrast, the zonal wind stress, and the strength of the maximum confluence normalized by the Coriolis parameter. In the scaling of γ_{wind}, Ro = α/f. For all of the runs, a horizontal resolution of $\Delta x = \Delta y = 1$ km is used, except for run 20 in which the resolution is $\Delta x = \Delta y = 0.5$ km.

Run	$\Delta_y\rho$ (kg m^{-3})	τ_x^w(N m^{-2})	α/f	$\gamma_{\text{wind}} = u_w^*/\text{Ro}\Delta u_g$
3	0.25	0	0.1	0
4	0.25	0.1	0.1	0.67
5	0.25	0.1	0.01	6.7
6	0.25	0.1	0.02	3.3
7	0.50	0.1	0.05	0.67
8	0.25	0.1	0	∞
9	0.25	0.01	0.1	0.21
10	0.25	0.05	0.1	0.47
11	0.25	0.028	0.1	0.35
12	0.476	0.1	0.1	0.35
13	0.476	0.037	0.1	0.21
14	0.25	0.025	0.02	1.65
15	0.25	0.1	0.19	0.35
16	0.166	0.1	0.1	1.00
17	0.25	0.0	0.02	0
18	0.25	0.25	0.1	1.05
19	0.25	0.1	0.03	2
20	0.25	0.1	0.1	0.67

erate wind stress of 0.1 N m^{-2}) are compared in Figs. 4, 5. For the frontogenesis-only run, the evolution of the zonally averaged density at both fronts is similar and is characterized by an intensification of the horizontal density gradient and a flattening of isopycnals under the action of the thermally direct ageostrophic circulation. This frontogenetically induced restratification is dramatically altered in the presence of wind forcing. At the front forced by down-front winds, in the center of the domain, frontogenetic restratification is overwhelmed by Ekman advection of denser water over light, causing the isopycnals to be nearly vertical in the Ekman layer. In contrast, at the front forced by up-front winds, Ekman advection augments frontogenetic restratification, resulting in a significant enhancement of the stratification at the base of the Ekman layer. These figures provide a qualitative picture of the relative effects of friction and frontogenesis in modifying the stratification. To quantify these effects, diagnostics for the evolution of the volume-averaged stratification and PV were performed and are described in the next section.

c. Diagnostics for the change in mean stratification

As was described in section 2, changes in the volume-averaged stratification

$$\Delta\overline{N}^2 \equiv \overline{N}^2 - \overline{N}^2|_{t=0}, \tag{25}$$

and PV (normalized by f)

$$\frac{\Delta\overline{q}}{f} \equiv \frac{1}{fV}\int_{\mathcal{V}} (q - q|_{t=0})\, dV, \tag{26}$$

are caused by friction, frontogenesis, diabatic processes, and advection. To quantify the contribution of each of these processes in the modification of the mean stratification, the following quantities were calculated: the frictional change in PV due to vertical mixing of momentum,

$$\text{FRIC}_v \equiv \frac{1}{fV}\int_0^t\int_{\mathcal{V}} \boldsymbol{\nabla}\times\mathbf{F}_v\cdot\boldsymbol{\nabla}b\, dV\, dt, \tag{27}$$

the frictional change in PV due to lateral mixing of momentum,[1]

$$\text{FRIC}_l \equiv \frac{1}{fV}\int_0^t\int_{\mathcal{V}} \boldsymbol{\nabla}\times\mathbf{F}_l\cdot\boldsymbol{\nabla}b\, dV\, dt, \tag{28}$$

the change in stratification due to frontogenesis,

$$\text{FRONT}_i \equiv \frac{1}{fV}\left[\left(\int_{\mathcal{A}}\zeta' b'\, dA|_{z=0,t} - \int_{\mathcal{A}}\zeta' b'\, dA|_{z=0,t=0}\right) - \left(\int_{\mathcal{A}}\zeta' b'\, dA|_{z=-D,t} - \int_{\mathcal{A}}\zeta' b'\, dA|_{z=-D,t=0}\right)\right], \tag{29}$$

(primes denote a deviation from the areal average) the change in PV due to diabatic processes,[2]

$$\text{DIA}_i \equiv \frac{1}{fV}\int_0^t\int_{\mathcal{V}} \boldsymbol{\omega}_a\cdot\boldsymbol{\nabla}\mathcal{D}\quad dV\, dt, \tag{30}$$

and the change in PV due to advection,

$$\text{ADV}_i \equiv -\frac{1}{fV}\int_0^t\int_{\mathcal{V}} \mathbf{u}\cdot\nabla q\, dV\, dt. \tag{31}$$

[1] The lateral mixing of momentum, $\mathbf{F}_l$, is associated with biharmonic friction, while vertical mixing of momentum comprises the remainder of the frictional force, i.e., $\mathbf{F}_v = \mathbf{F} - \mathbf{F}_l$ and was diagnosed from the KPP mixing scheme.

[2] The term encompassing diabatic processes, $\mathcal{D}$, includes both lateral mixing of buoyancy by biharmonic diffusion and vertical mixing as diagnosed from the KPP mixing scheme. It does not include implicit mixing associated with the advection scheme, which is accounted for in (31).

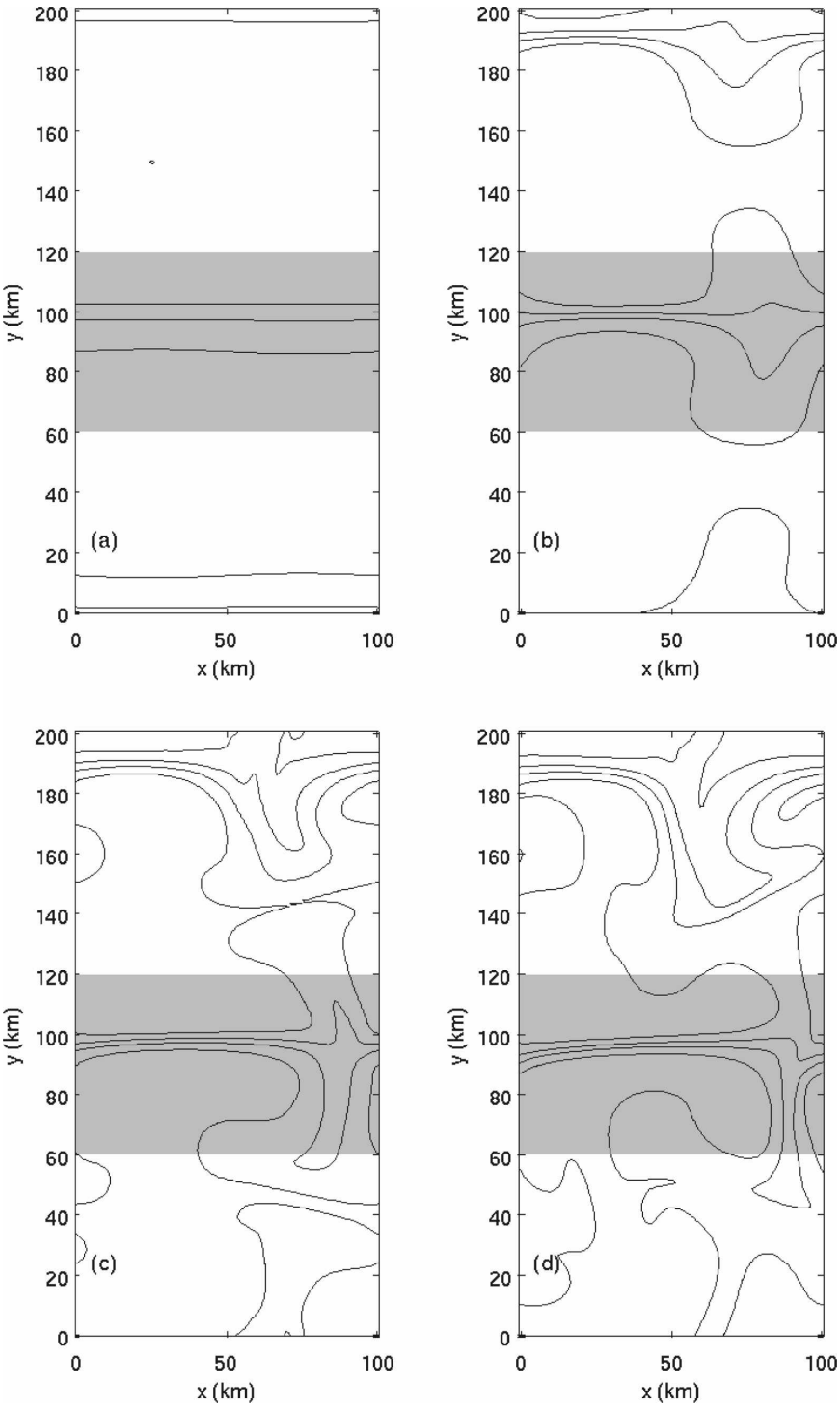

FIG. 3. Evolution of density at $z = 0$ for run 4. Contours of density with a contour interval of 0.08 kg m^{-3} are shown for $t =$ (a) 0.1, (b) 2.6, (c) 5.1, and (d) 7.6 inertial periods. The region shaded in gray denotes domain 1 used in the PV budget. Domain 2 encompasses the rest of the model domain.

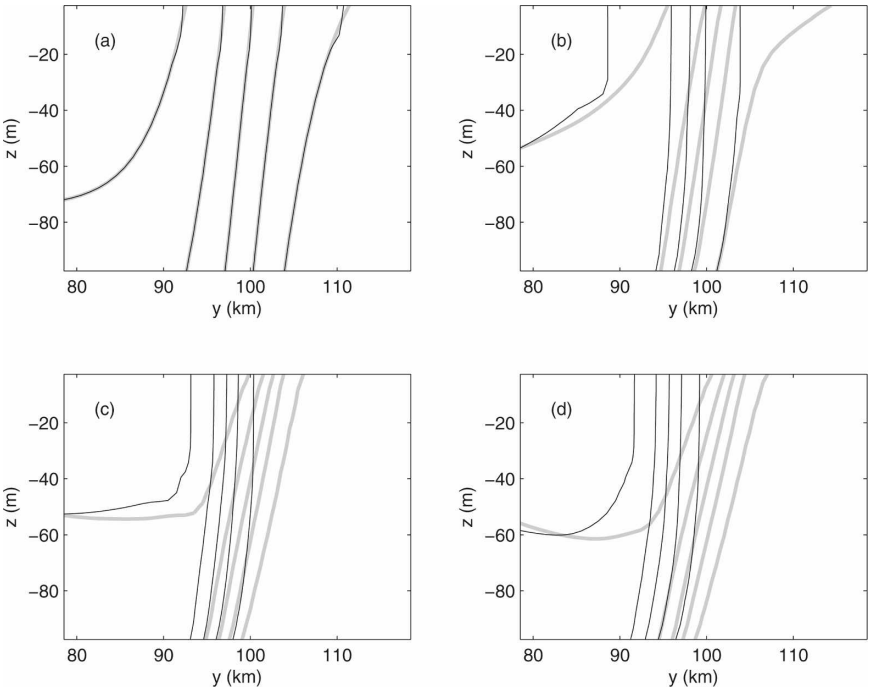

FIG. 4. Zonally averaged density field near the front in the center of the domain for run 3 (thick gray) and run 4 (black) at times (a) 0.1, (b) 2.6, (c) 5.1, and (d) 7.6 inertial periods. The contour interval is 0.05 kg m^{-3}.

For convenience (26), (27), (28), (30), and (31) have been normalized by f so as to be expressed in units of stratification, so that

$$\Delta\overline{N}^2 = \mathrm{FRONT}_i + \frac{\Delta\overline{q}}{f} = \mathrm{FRONT}_i + \mathrm{FRIC}_\nu + \mathrm{FRIC}_l + \mathrm{DIA}_i + \mathrm{ADV}_i. \tag{32}$$

Note that in calculating the terms in the PV budget (27), (28), (30), and (31), Gauss's theorem has not been applied, but instead a volume integral of the PV equation

$$\frac{\partial q}{\partial t} = -\mathbf{u}\cdot\boldsymbol{\nabla} q + \boldsymbol{\omega}_a\cdot\boldsymbol{\nabla}\mathcal{D} + \boldsymbol{\nabla}\times\mathbf{F}\cdot\boldsymbol{\nabla} b \tag{33}$$

has been used because this is easier to evaluate numerically. In the diagnostic calculations, two control volumes were used, one encompassing the front in the center of the domain (referred to as domain 1) and the other occupying the rest of the domain (domain 2). Both volumes extend to the bottom, remain fixed in time, and are indicated in Fig. 3.

Time series of changes in the mean stratification and PV and terms (27)–(31) are plotted in Fig. 6 for run 4. In domain 1, the mean PV initially decreases, as is expected for a front forced by down-front winds. However, because of frontogenesis, the decrease in mean stratification is slower than that of PV (Fig. 6a), that is, $\Delta\overline{N}^2 - \Delta\overline{q}/f = \mathrm{FRONT}_i > 0$. The bulk of the decrease in the volume-averaged PV is due to *vertical* friction, FRIC_ν, with diabatic processes, DIA_i, resulting in PV reduction as well (Fig. 6c). In contrast, *lateral* friction and advection of PV contribute to increasing the mean PV in domain 1.

After several inertial periods, both FRIC_ν and FRONT_i asymptote to nearly a constant value, indicating that not only is frontogenesis arrested but that some process limits erosion of PV by winds. The mechanism by which PV removal by down-front winds is suppressed will be described below, but first the strengths of frontogenetic restratification versus frictional destratification will be compared. Averaged over the last two inertial periods of the experiment, FRIC_ν contributes to a reduction in $\Delta\overline{q}/f$ by an amount $2.3\times10^{-6}\ \mathrm{s}^{-2}$, more than double the $9.9\times10^{-7}\ \mathrm{s}^{-2}$ increase in stratification by FRONT_i, suggesting that frictional PV change is not only comparable in magnitude to frontogenetic restratification but actually the dominant of the two processes.

Frictional reduction of PV is eventually suppressed because of a partial cancellation of the imposed wind stress by the geostrophic stress [e.g., (11)], which is en-

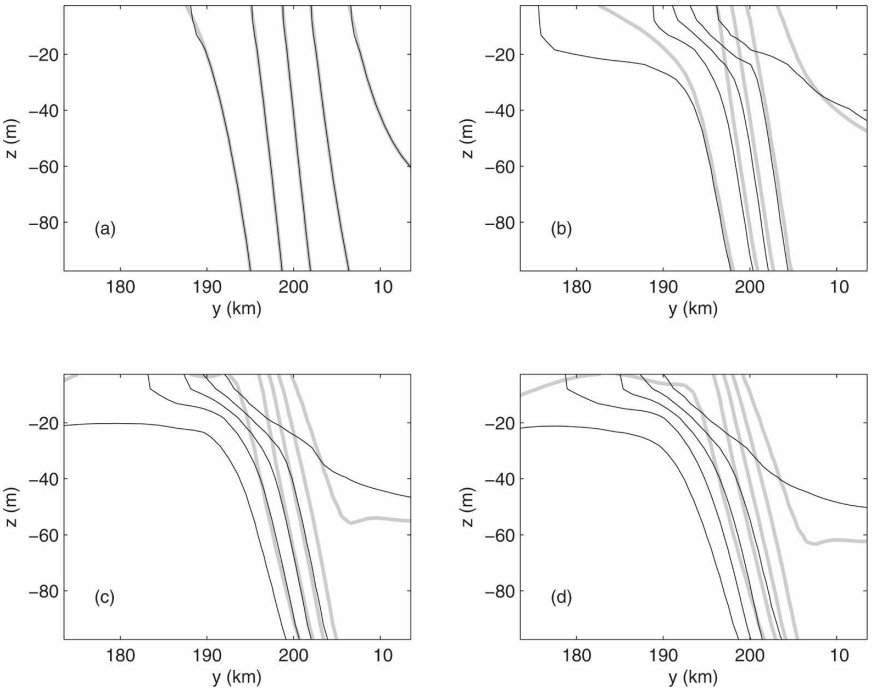

FIG. 5. Same as Fig. 4, but for the front on the edges of the domain.

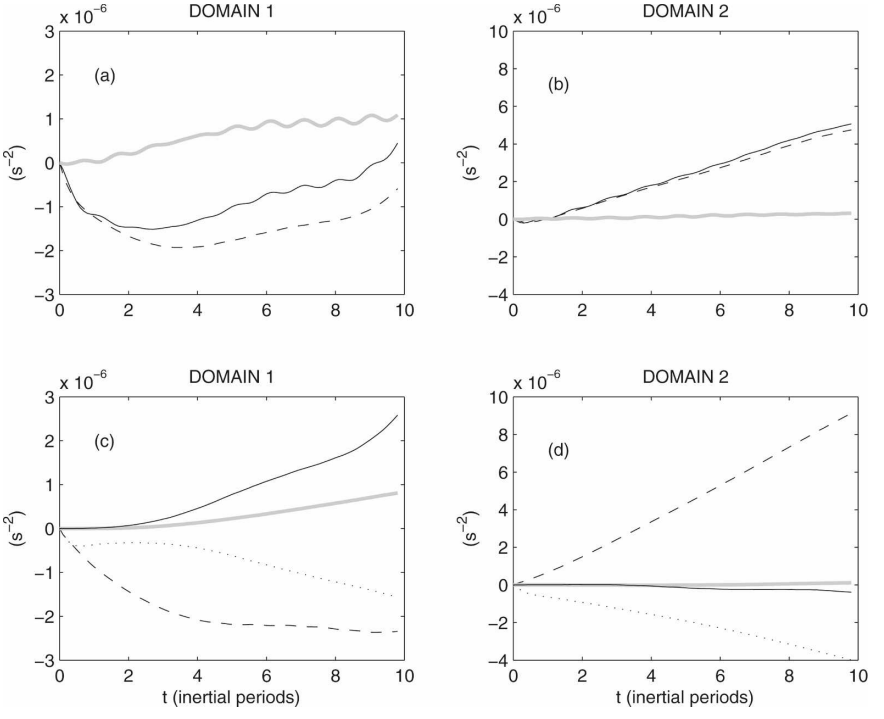

FIG. 6. Temporal change in the mean PV and stratification; and the processes that give rise to this change as diagnosed from run 4. (a), (b) The change in mean stratification, $\Delta\overline{N}^2$ (thin black) and PV, $\Delta\overline{q}/f$ (dashed) are plotted along with the frontogenetic contribution to re-stratification, FRONT_i (thick gray), for domains 1 and 2, respectively. (c), (d) The change in PV due to vertical friction, FRIC_ν (dashed), lateral friction, FRIC_l (thick gray), diabatic processes, DIA_i (dotted), and advection, ADV_i (thin black), are plotted for domains 1 and 2, respectively.

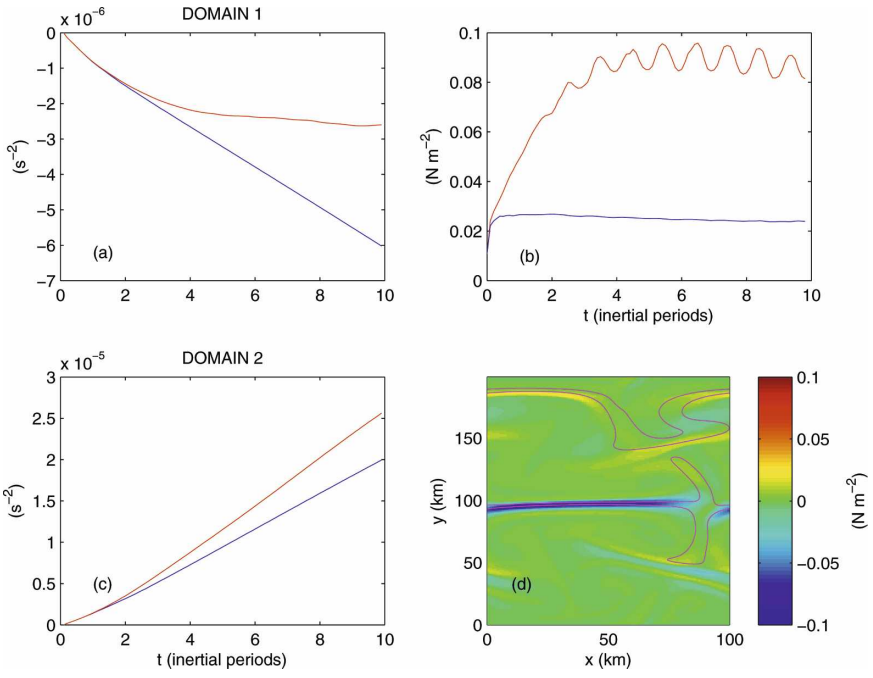

FIG. 7. Surface integral of the vertical frictional PV flux for run 8 (blue) and run 4 (red), for domains (a) 1 and (c) 2. (b) Time series of the maximum absolute value of the zonal component of the geostrophic stress τ_x^g for run 8 (blue) and run 4 (red). (d) The density field (magenta contours of interval 0.1 kg m^{-3}) and τ_x^g (shades) for run 4 at $t = 6.5$ inertial period.

hanced through frontogenesis (Fig. 7). Comparing time series of the maximum geostrophic stress in runs 4 and 8 (which was forced by winds only), reveals that frontogenesis, through intensifying the geostrophic shear, strengthens τ_x^g to such a degree that it becomes comparable in magnitude to the wind stress (Fig. 7b). At the front in domain 1, τ_x^g opposes the wind stress, while near the front in domain 2 it reinforces the wind forcing. This behavior reveals a coupling between frontogenesis and frictional processes that leads to an augmentation of frictional injection of PV in domain 2 and a quelling of PV removal by down front winds.

It might be argued that because frontogenesis is arrested by horizontal mixing in the simulations, frontogenetic restratification is repressed, and hence its effect is underestimated (although our simulations are not unique in this respect because all numerical simulations of ocean fronts have some form of explicit or implicit lateral mixing that arrests frontogenesis to some degree). To address this issue, FRIC$_\nu$ and FRONT$_i$ from run 4 are compared to the amount of restratification that would occur if frontogenesis could continue to the point of the formation of a discontinuity in density. The derivation for this upper bound on frontogenetic restratification is given in appendix A, Eq. (A1). Given the cross front buoyancy contrast $\Delta b = 2.4 \times 10^{-3}$ m s^{-2}, depth of the layer $H = 100$ m, width of domain 1 $L_y = 60$ km, and estimate for the displacement of the front from its initial location, $Y \approx 3$ km (based on solutions from run 3; see Fig. 4), the maximum restratification by frontogenesis for run 4 in domain 1 is $\Delta\overline{N}^2_{\text{front}} \approx 2.4 \times 10^{-6}$ s^{-2}. This restratification is between 2 and 3 times greater than FRONT$_i$ and approximately equal to the destratification by FRIC$_\nu$ at the end of experiment 4. Hence, even if frontogenesis could continue to frontal collapse, the resulting stratification would be at most comparable to that removed by friction, emphasizing the importance of PV destruction by down-front winds in the modification of the mixed layer stratification.

In domain 2, where the winds are up front, frictional PV creation completely dominates over frontogenetic restratification (Figs. 6b,d). Both mean stratification and PV increase throughout the duration of the experiment and are almost indistinguishable from one another, evidencing the negligible effect of frontogenesis on the mean stratification. In this case, nearly all of the increase in mean PV and stratification is associated with vertical friction, while diabatic processes and advection lead to a slight reduction in PV.

The difference between FRIC$_\nu$ in the two domains attests to an asymmetry between the efficiency of PV

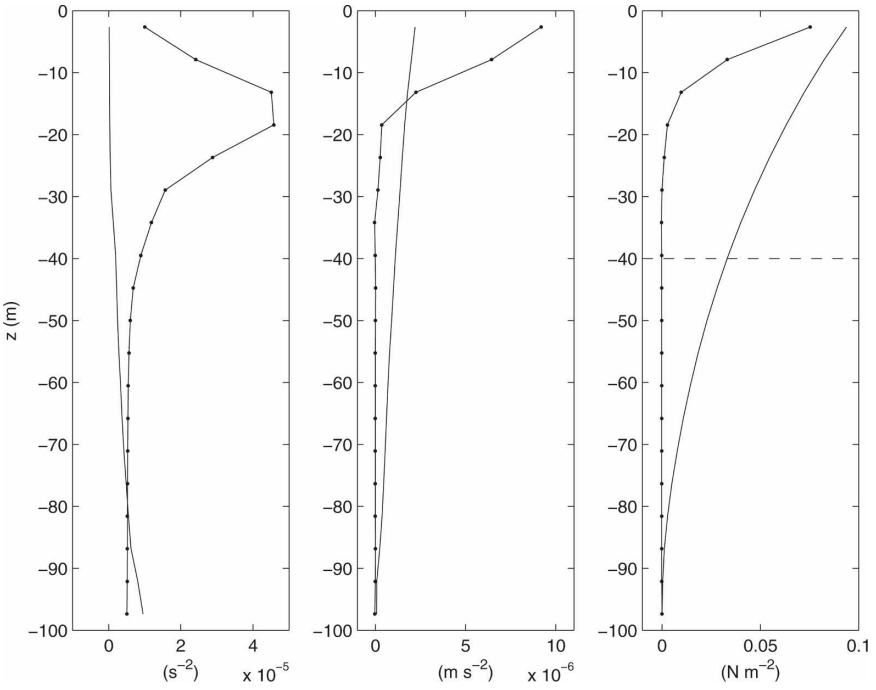

FIG. 8. Comparison of the stratification, zonal friction force F_x and zonal stress $\rho_o \int_{-D}^{z} F_x dz$ in domains 1 and 2 averaged between $t = 2 - 3$ inertial periods for run 4. (left) Square of the buoyancy frequency, (middle) zonal frictional force, and (right) zonal stress averaged over frontal regions where the magnitude of the zonally averaged N–S buoyancy gradient at the surface exceeded 3.5×10^{-8} s^{-2}, for domains 1 (solid) and 2 (dotted). The scaling for the depth of the Ekman layer $0.4u_w^*/f$ (dashed line) is indicated in the right panel.

injection and removal by up- and down-front winds.[3] As shown in Fig. 8, most of this asymmetry is due to the fact that as up front winds restratify the fluid, the turbulent stress is confined to a depth shallower than the Ekman layer. In contrast, stress induced by down front winds is felt through the entire weakly stratified Ekman depth $\delta_e = 0.4u_w^*/f$. Reducing the depth over which the stress is distributed enhances the frictional force, Ekman flow, differential horizontal advection of buoyancy, and hence frictional change in stratification. In addition, the suppression (augmentation) of frictional removal (injection) of PV by the geostrophic stress described above contributes to the asymmetric response to up and down front wind forcing.

d. Sensitivity to forcing and flow parameters

In the previous section it has been shown that for fronts forced by the relatively strong confluence ($\alpha = 0.1f$) and moderate winds ($\tau_x^w = 0.1$ N m^{-2}) of run 4, friction played a greater role than frontogenesis in the change of mean stratification in the mixed layer. To assess the sensitivity of this result to the forcing and flow parameters, a suite of experiments was performed in which α, τ_w^w, and $\Delta\rho$ were varied (e.g., Table 1). The metric used to determine the relative contributions of friction and frontogenesis to the re–de-stratification of the mixed layer is the same as has been used in the previous section, that is, the ratio FRIC_ν to FRONT_i averaged over the last two inertial periods of each experiment. The absolute value of this quantity is plotted in Fig. 9 against the scaling γ_{wind}.[4] As in run 4, for all of

[3] Notice that this asymmetry is even more pronounced than what can be inferred from Figs. 6c,d. A fair comparison between the amount of PV injected and removed in domains 2 and 1 entails calculating the relative contributions of FRIC_ν in each domain to the volume-integrated PV of the whole model domain, which involves multiplying FRIC_ν by f times the volume of the respective domains. Consequently, the relative importance of frictional injection to removal of PV is greater than that seen in the figure by a factor of 2.3, i.e., the ratio of the volumes of domain 2 to 1.

[4] Note that γ_{wind} and $\text{FRIC}_\nu/\text{FRONT}_i$ averaged over the last two inertial periods are not measures of the exact same quantity: one scales the relative rates of re/destratification while the other is a measure of the relative total change in stratification. However, because the time dependence of FRIC_ν and FRONT_i seen in the experiments is not too different from being linear, $\text{FRIC}_\nu/\text{FRONT}_i$ is a representative metric of the relative rates of stratification increase/decrease, and hence it can be compared to γ_{wind}.

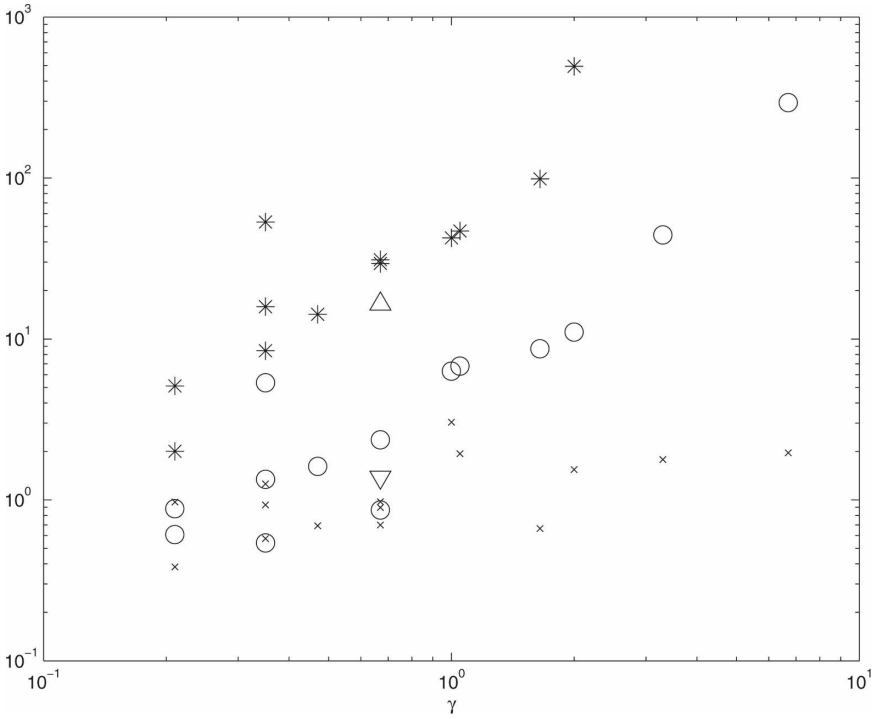

FIG. 9. The absolute value (y axis) of the ratio of term FRIC_ν to FRONT_i averaged over the last two inertial periods of the experiment vs $\gamma_{\mathrm{wind}} = u_w^*/\mathrm{Ro}\Delta u_g$ for all of the runs forced by both winds and confluence. Asterisks and circles correspond to values taken from domains 2 and 1, respectively. Results from run 20, where the resolution was doubled, are given by the upward (domain 2) and downward (domain 1) triangles. The ratio of $|\mathrm{FRIC}_\nu|$ in domain 1 (averaged over the last two inertial periods) to the scaling for the upper bound on the restratification by frontogenesis $\Delta\overline{N}^2_{\mathrm{front}}$ is denoted by the xs.

the experiments, frictional injection of PV by the up-front winds in domain 2 was stronger than frictional removal of PV in domain 1. Restratification by friction ranged from being 2 to ~500 times greater than frontogenic restratification in domain 2, while destratification by down-front winds exceeded FRONT_i for the majority of the experiments, except for runs where $\gamma_{\mathrm{wind}} < 1$ and the density contrast was large (i.e., runs 7, 12, and 13). In both domains, the ratio of FRIC_ν to FRONT_i generally increased with γ_{wind}, indicating that the scaling arguments presented in section 5 have some skill in predicting the dependence of the basic features of re–de-stratification at wind- and strain-forced fronts on the key parameters involved. However, the scaling did not predict the asymmetric response to up and down front wind forcing. This is to be expected because in deriving γ_{wind}, it was assumed that the wind stress was distributed over the turbulent Ekman depth for both down and up front winds, whereas, as illustrated in Fig. 8, the stress is confined to a shallower depth for up front winds as a consequence of the stratification.

The arrest of frontogenesis by horizontal mixing does not affect the general result that friction is at least as important as frontogenesis in the modification of the stratification. In run 20, where the horizontal resolution was enhanced and the biharmonic diffusivity–viscosity was reduced, $|\mathrm{FRIC}_\nu/\mathrm{FRONT}_i| > 1$, as in the equivalent lower-resolution run. In addition, the ratio $\mathrm{FRIC}_\nu/\mathrm{FRONT}_i|$ calculated using the upper bound on frontogenetic restratification, (A1), and FRIC_ν from domain 1 is never much smaller than one for any of the experiments, which suggests that the importance of friction in the dynamics of the stratification of the upper ocean is a robust result.

7. Discussion

In the previous sections, the focus has been on quantifying changes in the vertically averaged stratification of the surface mixed layer generated by tilting a baroclinic buoyancy front via frictionally and frontogenetically driven ageostrophic flows. In this section, it is shown that the changes in PV and stratification induced by friction and frontogenesis penetrate to different depths into the upper ocean.

Frictional flows driven by spindown and up-front

winds restratify the water column within the Ekman boundary layer depth. A layer of enhanced stratification confined to the surface Ekman layer is well visible in all panels of Fig. 5. Down-front winds, instead, destratify the water column, and their destabilizing effect is felt all the way down to the mixed layer base as shown in Fig. 4 and can penetrate into the pycnocline through the formation of intrathermocline eddies (Thomas 2008).

Restratification by frontogenesis occurs over the depth H of the frontogenesis-driven ASC. In appendix B, it is shown that if the Q vector is confined to a region of width $\mathcal{L}$, chosen to represent the frontal width, and the background vertical stratification N_o is constant, then $H \sim \mathcal{L}f/N_o$ is a good measure of the vertical extent of the restratifying, frontogenesis-driven ASC. When the stratification is not constant but has a mixed layer of thickness $h_{\rm ml}$ with stratification $N_{\rm ml}$ above a thermocline with stratification $N_{\rm tc}$, the penetration depth and strength of frontogenesis will be affected. As shown by Boccaletti et al. (2007), the presence of a mixed layer in a baroclinic current allows for the growth of submesoscale, shallow baroclinic instabilities whose horizontal flow can be frontogenetic. The geostrophic forcing associated with these mixed layer instabilities (MLI) is limited to the depths of the weakly stratified surface layer (i.e., $h \sim h_{\rm ml}$, which for the Burger number Bu $\sim$ 1 implies that the horizontal length scale of the Q vector scales with the mixed layer Rossby radius: $\mathcal{L}_{\rm ml} \sim N_{\rm ml}h_{\rm ml}/f$. For such situations, solutions to the Eliassen–Sawyer equation in (12) are nearly completely confined to the mixed layer because there is very little penetration of the ASC into the thermocline because of the large difference in stratification. In this case, a good measure for H is the mixed layer depth $H \approx h_{\rm ml}$. For the case of deep fronts that penetrate into the thermocline and that are forced by mesoscale eddies and meanders, the vertical scale of the frontogenesis-driven ASC scales with the thermocline depth given by $H \sim \mathcal{L}_d f/N_{\rm tc}$, where $\mathcal{L}_d$ is the deformation radius associated with the mesoscale straining flow.

The strength of the frontogenesis-driven restratifying ageostrophic flow is also affected by the presence of a mixed layer for two reasons: 1) the magnitude and horizontal scale of the Q vector differ for MLI and mesoscale eddies and 2) the stratification affects the magnitude of the overturning streamfunction. A scaling for the relative strengths of the ageostrophic flows driven by frontogenesis for MLI and mesoscale eddies can be constructed from (B1), that is,

$$\frac{\Psi_z^{\rm MLI}}{\Psi_z^{\rm meso}} \sim \frac{Q_o^{\rm MLI}}{Q_o^{\rm meso}} \frac{N_{\rm tc}\mathcal{L}_{\rm ml}}{N_{\rm ml}\mathcal{L}_d}. \tag{34}$$

The Rossby numbers characteristic of submesoscale MLI are larger than those associated with mesoscale eddies, suggesting that submesoscale straining dominates over mesoscale confluence. Cross-front density gradients typically intensify moving from the thermocline to the surface. Both of these flow characteristics will conspire to make $Q_o^{\rm MLI}/Q_o^{\rm meso} \gg 1$. However, the deformation radius of mesoscale eddies is much larger than the mixed layer Rossby radius of deformation so that for typical conditions, $(N_{\rm tc}\mathcal{L}_{\rm ml})/(N_{\rm ml}\mathcal{L}_d) \sim h_{\rm ml}/h_{\rm tc} \ll 1$. This scaling argument suggests that for oceanic flows where both MLI and deep mesoscale strain is present, frontogenesis-driven ageostrophic flows associated with both mechanisms will be of similar strength. Having said this, frontogenesis by MLI will be faster than that driven by mesoscale eddies because the time scale of frontogenesis goes as the inverse of the strain rate, and hence as ${\rm Ro}^{-1}f^{-1}$. However it is likely that mesoscale frontogenesis remains important on long time scales for restratification below the mixed layer base. Numerical simulations that resolve both mesoscale and submesoscale instabilities are needed to settle the issue.

Finally, the ageostrophic circulations associated with MLIs are very fast and redistribute material properties within the whole mixed layer on the order of a day. In particular, Boccaletti et al. (2007) find that the enhanced stratification resulting from surface friction in the Ekman layer is rapidly communicated to the rest of the mixed layer. Hence, in the real ocean any change of PV and stratification in the Ekman layer is likely to be felt throughout the whole mixed layer as a result of three-dimensional instabilities not considered in this paper.

8. Conclusions

Traditional models of turbulent boundary layers at the ocean surface assume that the buoyancy and momentum budgets are essentially one-dimensional; that is, stratification and shears are set through turbulent downward transport of fluxes and stresses applied at the air–sea interface. This description is appropriate as long as buoyancy at the surface ocean is horizontally homogeneous. In practice, however, the ocean boundary layers are populated with lateral fronts that profoundly affect the vertical mixing of tracers and momentum. Lapeyre et al. (2006) show that frontogenetic slumping of density gradients effectively restratifies the ocean surface even without any air–sea flux. In this paper, it was shown that frictional forces acting on baroclinic currents are also effective at increasing–reducing the stratification beyond what a one-dimension-

al budget would predict. Friction modifies the stratification of a rotating fluid through two different processes: stretching and squeezing of the water column induced by horizontal variations of the frictional forces and Ekman advection of the lateral stratification, the latter of which is illustrated in Fig. 1. Simple scaling arguments and numerical simulations suggest that for typical ocean conditions, Ekman advection is as important or more important as frontogenesis at modifying the stratification of the mixed layer.

Numerical simulations support the simple scaling analysis but further reveal that there is asymmetry in the changes of stratification when the wind forcing is oriented up or down front (i.e., directed against or with the frontal shear). Up front wind restratification is typically larger than down wind front destratification for equal wind stress. Two effects contribute to the asymmetry. First, stratification generated by up front winds leads to a reduction in vertical penetration depth of the turbulent stress and hence an enhancement of the frictional force and stratification change relative to that associated with the down front wind forcing. Second, the frictional destratification is reduced over restratification because the inherent spindown of a baroclinic geostrophic flow always tends to increase the PV of the fluid, and hence counteracts the destratifying tendency of down front winds. This effect is accentuated by frontogenesis because the surface frictional stress ascribable to geostrophic shear that drives spindown is amplified during frontal intensification.

A question arises as to whether the effect of friction is overemphasized by ignoring the compensation between the restratification driven by up front winds and the destratification resulting from down front winds. Satellite observations show that the orientation of fronts at the ocean surface is nearly isotropic at small scales, suggesting that up wind and down wind conditions (as well as fronts with intermediate orientation) might occur roughly with the same frequency (e.g., Castelao et al. 2006). The compensation between the surface PV fluxes over many fronts, however, does not imply that the oceanic response to these fluxes averages out as well. For example, the ocean response to the diurnal cycle of heating and cooling is very asymmetric, even though the daytime generation of PV is largely compensated by PV destruction at night: daily heating restratifies mostly in a thin surface boundary layer, while nighttime cooling penetrates down to the mixed layer base. Similarly, the generation of high PV by up front winds concentrates stratification within the surface Ekman layer, while destruction of PV by down front winds triggers convection and reduces stratification all the way to the mixed layer base. Thomas (2007) shows that the low PV anomalies generated through convection are eventually subducted into the ocean interior as intrathermocline eddies, while the high PV anomalies remain at the surface. Hence, winds generate positive PV anomalies close to the ocean surface and negative PV anomalies in the thermocline and the effects of up front and down front winds do not cancel out despite the compensation in surface PV fluxes. This PV redistribution is likely to occur in the real ocean, because the scaling arguments and numerical simulations described here suggest that wind-driven PV forcing is a leading-order process in setting the PV of the upper ocean. A detailed study of the oceanic response to a variable and compensating PV flux is left for future work.

The importance of frictional forces in setting the stratification of the global ocean should not come as a surprise. Frictional forces and diabatic processes are ultimately the only processes that can generate and destroy stratification. Frontogenesis and advection can only redistribute the stratification. Hence, the steady-state stratification of the upper ocean is maintained by a balance of frictional and diabatic fluxes. Frontogenesis and advection regulate how the stratification generated/destroyed at the surface is redistributed in the vertical. Only during transient events can any one process dominate over the others. The surprise is that lateral fronts can substantially modify the surface fluxes that enter in the ocean. This modulation occurs at frontal scales between tens of kilometers and hundreds of meters, which are typically subgrid in ocean models used for climate studies. It is therefore an open question: What is the role of frontogenetic and frictional processes in maintaining the observed ocean mean state?

The scaling arguments described in this paper focus primarily on two-dimensional flows. In three dimensions, submesoscale instabilities can develop along mixed layer fronts that act to slump outcropping fronts (Boccaletti et al. 2007). The numerical simulations described in this paper were deliberately configured to suppress frontal instabilities by imposing large steady strain fields (Bishop 1993; Spall 1997) and strong winds aligned with the fronts (Thomas 2005). Frontal instabilities, however, developed if the strain field or the winds were substantially reduced (not shown). Boccaletti et al. (2007) and Capet et al. (2008) show that submesoscale instabilities develop when strain and winds are not steady. These instabilities might play an important role in setting the mixed layer stratification, because they are associated with overturning circulations

that restratify the surface mixed layer and subduct surface waters into the ocean interior. The details of the exchange of waters between the mixed layer and the interior are not well understood. For example, Lapeyre et al. (2006) argue that frontogenetic ASC associated with the mesoscale straining field can also be important and compete with ASC generated by instabilities within the mixed layer. We plan to investigate the dynamics of these three-dimensional circulations and their effect on the mean stratification of the ocean in future work.

A final comment pertains to the implication of frictional re–de-stratification for numerical models. The scaling arguments presented above suggest that to accurately simulate the stratification in the upper ocean using numerical models, wind-driven frictional processes should be accounted for. If a numerical model does not resolve the Ekman layer, frictional re/destratification will be underestimated. The strength of the Ekman velocity is proportional to the frictional force. The frictional force at the top grid point of a numerical model, using a simple centered difference approximation, is

$$F = \frac{1}{\rho_o}\frac{\partial \tau}{\partial z} \approx \frac{(\tau^w) - \tau|_{z=-\Delta z}}{\rho_o \Delta z}. \tag{35}$$

The turbulent stress in a fluid decays with depth, approximately going to zero for depths beneath the Ekman layer. If the top grid of a numerical model is thicker than the Ekman layer, this suggests that $\tau|_{z=-\Delta z} \approx 0$, and (35) is $F \approx (\tau^w)/\Delta z$, which compared to the appropriate scaling for the frictional force $F \sim \tau^w/\rho_o\delta_e$, is smaller by a factor of $\delta_e/\Delta z$. This argument implies that a numerical model that does not resolve the Ekman layer, ratio (21) will be reduced by a factor of $\delta_e/\Delta z$ and the impact of friction on modifying the stratification will be artificially reduced. To avoid this pitfall, numerical models should use mesh grids with a vertical resolution smaller than the Ekman layer depth at the boundaries.

Acknowledgments. This research was supported by NSF Grants OCE-0549699 and OCE-0612058 (L.T.) and OCE-0612143 (R.F). We thank Baylor Fox-Kemper and Patrice Klein for useful discussions.

APPENDIX A

Bounds on the Change in Stratification by Frontogenesis

An upper bound on the stratification increase due to frontogenesis can be calculated. Frontogenesis will proceed until frontal collapse—that is, until the buoyancy forms a discontinuity. After this point, frontogenesis will not drive further restratification. At the time of frontal collapse, the location of the maximum buoyancy gradient will be displaced relative to its initial location by a distance Y; for example, in the solution of Hoskins and Bretherton (1972) the front is shifted to the cyclonic side of the front. If, for example, the initial buoyancy field had a negative buoyancy gradient in the y direction and was centered at $y = 0$ and stays approximately two-dimensional, then at frontal collapse the surface and bottom buoyancy will take the form $b|_{z=0} = \Delta b[\mathcal{H}(y - Y) - 1]$ and $b|_{z=-H} = \Delta b[\mathcal{H}(y + Y) - 1]$, where $\mathcal{H}$ is the Heaviside step function and $\Delta b > 0$ is the buoyancy contrast crossing the front. Substituting these expressions into (1) to calculate the maximum mean stratification increase that can be attained through frontogenesis, one finds

$$\Delta\overline{N^2_{\text{front}}} = 2\frac{\Delta b Y}{H L_y}. \tag{A1}$$

It is difficult to determine analytically how the displacement Y of the maximum frontal gradient depends on the key parameters of the problem because it is a quantity that is set during the nonlinear evolution of the front. Having said this, it can be stated with certainty that Y will be less than the initial width of the front, L_f, because confluence and convergence during frontogenesis will always push the isopycnals comprising the frontal interface toward the center of confluence. With this upper bound on Y, it can be deduced that

$$\Delta\overline{N^2_{\text{front}}} < 2\frac{\Delta b}{H}\frac{L_f}{L_y}.$$

APPENDIX B

Vertical Extent of Frontogenetic Ageostrophic Secondary Circulations

The Eliassen–Sawyer equation in (12) can be used to compute the vertical penetration H of the frontogenesis-driven ASC. As an illustrative example, the problem is solved using an idealized form of the stratification and Q vector. Consider a Q vector that has a periodic lateral structure: $Q_2 = \Re[Z(z)e^{i2\pi y/\mathcal{L}}]$, with a wavelength $\mathcal{L}$. With this form, the solution for the streamfunction is $\psi = \Re[\Psi(z)e^{i2\pi y/\mathcal{L}}]$ and (12) becomes $\Psi_{zz} - l^2N^2/f^2\Psi = -2Z/f^2$. Assuming that (1) the Q vector is confined to the surface over a depth h, (2) its vertical structure is approximated by a Heaviside step function, that is, $Z = Q_o$ = a constant for $z > -h$ and zero everywhere else, and (3) the stratification is constant, $N^2 = N_o^2$, then the solution for Ψ is

$$\Psi = \frac{2Q_o}{f^2\lambda^2}\begin{cases} (1-\cos\lambda z) + \dfrac{(1-\cos\lambda h - \sin\lambda h)}{(\cos\lambda h + \sin\lambda h)}\sin\lambda z & z > -h \\ \dfrac{(\cos\lambda h - 1)}{(\cos\lambda h + \sin\lambda h)}\, e^{\lambda(z+h)} & z < -h, \end{cases} \tag{B1}$$

where $\lambda = 2\pi N_o/f\mathcal{L}$. The key parameter for the vertical structure of the ASC is the Burger number $\mathrm{Bu} = N_o^2h^2/f^2\mathcal{L}^2 = \lambda^2h^2/(2\pi)^2$. Because the Q vector is generated by the geostrophic flow, both the Q-vector and geostrophic flow have similar Burger numbers. Geostrophic flows have Burger numbers that are typically of order one. For $\mathrm{Bu} = O(1)$, (B1) predicts that the ASC penetrates a finite distance beneath the region of forcing, decaying to 10% of its maximum value at $z \approx -1.25\,h$, indicating that the vertical scale $h \sim \mathcal{L}f/N_o$ is a good measure of the vertical extent H of the restratifying, frontogenesis-driven ASC.

REFERENCES

Adamson, D. S., S. E. Belcher, B. J. Hoskins, and R. S. Plant, 2006: Boundary layer friction in midlatitude cyclones. *Quart. J. Roy. Meteor. Soc.,* **132,** 101–124.

Bishop, C. H., 1993: On the behaviour of baroclinic waves undergoing horizontal deformation. II: Error-bound amplification and rossby wave diagnostic. *Quart. J. Roy. Meteor. Soc.,* **119,** 241–267.

Boccaletti, G., R. Ferrari, and B. Fox-Kemper, 2007: Mixed layer instabilities and restratification. *J. Phys. Oceanogr.,* **37,** 2228–2250.

Capet, X., J. McWilliams, M. Molemaker, and A. Shchepetkin, 2008: Mesoscale to submesoscale transition in the California Current System. Part II: Frontal processes. *J. Phys. Oceanogr.,* **38,** 44–64.

Castelao, R. M., L. P. Mavor, J. A. Barth, and L. C. Breaker, 2006: Sea surface temperature fronts in the California Current System from geostationary satellite observations. *Geophys. Res. Lett.,* **111,** C09026, doi:10.1029/2006JC003541.

Cooper, I. M., A. J. Thorpe, and C. H. Bishop, 1992: The role of diffusive effects on potential vorticity in fronts. *Quart. J. Roy. Meteor. Soc.,* **118,** 629–647.

Davis, C. A., M. T. Stoelinga, and Y. H. Kuo, 1993: The integrated effect of condensation in numerical simulations of extratropical cyclogenesis. *Mon. Wea. Rev.,* **121,** 2309–2330.

Fox-Kemper, B., R. Ferrari, and R. Hallberg, 2008: Parameterization of mixed layer eddies. I: Theory and diagnosis. *J. Phys. Oceanogr.,* **38,** 1145–1165.

Garrett, C. J. R., and J. W. Loder, 1981: Dynamical aspects of shallow sea fronts. *Philos. Trans. Roy. Soc. London,* **A302,** 563–581.

Haine, T., and J. C. Marshall, 1998: Gravitational, symmetric, and baroclinic instability of the ocean mixed layer. *J. Phys. Oceanogr.,* **28,** 634–658.

Hoskins, B. J., and F. P. Bretherton, 1972: Atmospheric frontogenesis models: Mathematical formulation and solution. *J. Atmos. Sci.,* **29,** 11–37.

——, I. Draghici, and H. C. Davies, 1978: A new look at the ω-equation. *Quart. J. Roy. Meteor. Soc.,* **104,** 31–38.

Lapeyre, G., P. Klein, and B. L. Hua, 2006: Oceanic restratification forced by surface frontogenesis. *J. Phys. Oceanogr.,* **36,** 1577–1590.

Large, W. G., J. C. McWilliams, and S. C. Doney, 1994: Oceanic vertical mixing: A review and a model with a nonlocal boundary layer parameterization. *Rev. Geophys.,* **32,** 363–403.

Marshall, J. C., and A. J. G. Nurser, 1992: Fluid dynamics of oceanic thermocline ventilation. *J. Phys. Oceanogr.,* **22,** 583–595.

Smolarkiewicz, P. K., and L. G. Margolin, 1998: Mpdata: A finite-difference solver for geophysical flows. *J. Comput. Phys.,* **140,** 459–480.

Spall, M., 1997: Baroclinic jets in confluent flow. *J. Phys. Oceanogr.,* **27,** 381–402.

Thomas, L. N., 2005: Destruction of potential vorticity by winds. *J. Phys. Oceanogr.,* **35,** 2457–2466.

——, 2007: Dynamical constraints on the extreme low values of the potential vorticity in the ocean. *Proc. 15th 'Aha Huliko 'a Hawaiian Winter Workshop,* Honolulu, HI, University of Hawaii at Manoa, 117–124.

——, 2008: Formation of intrathermocline eddies at ocean fronts by wind-driven destruction of potential vorticity. *Dyn. Atmos. Oceans,* **45,** 252–273, doi:10.1016/j.dynatmoce.2008.02.002.

——, and P. B. Rhines, 2002: Nonlinear stratified spin-up. *J. Fluid Mech.,* **473,** 211–244.

Thompson, L., 2000: Ekman layers and two-dimensional frontogenesis in the upper ocean. *J. Geophys. Res.,* **105,** 6437–6451.

Wimbush, M., and W. Munk, 1970: The benthic boundary layer. *The Sea,* A. E. Maxwell, Ed., Vol. 4, Wiley Interscience, 731–758.